International Journal of Applied Mechanics
Vol. 6, No. 1 (2014) 1450005 (17 pages)

DOI: 10.1142/S1758825114500057

Imperial College Press
www.icpress.co.uk

# FINITE ELEMENT ANALYSIS OF THE INTERFACE/SURFACE EFFECT ON THE ELASTIC WAVE BAND STRUCTURE OF TWO-DIMENSIONAL NANOSIZED PHONONIC CRYSTALS

WEI LIU*,†, YONGQUAN LIU†, XIANYUE SU†,‡ and ZHENG LI†

*College of Petroleum Engineering
China University of Petroleum
Beijing 102249, China

†Department of Mechanics and Aerospace Engineering
College of Engineering, Peking University
Beijing 100871, China
‡xyswsk@pku.edu.cn

Received 30 September 2013
Revised 12 November 2013
Accepted 12 November 2013
Published 30 January 2014



In this paper, an interface/surface element is formulated based on the Gurtin–Murdoch interface/surface elasticity theory for accounting the interface/surface effect on the elastic wave propagation in two-dimensional nanosized phononic crystals. The interface/surface element is subsequently incorporated into the finite element procedure for calculating the elastic wave band structure of two-dimensional nanosized phononic crystals with consideration of the interface/surface effect. Elastic wave band structures of two-dimensional phononic crystals comprising a square array of circular or elliptical cylindrical nanoholes embedded in an aluminum matrix are analyzed. Numerical results evidence that the interface/surface effect on the elastic wave band structure can be remarkable when the characteristic size reduces to nanometers.

*Keywords*: Phononic crystals; band structure; interface/surface effect; finite element method.

## 1. Introduction

Phononic crystals (PCs), which are artificial composites bearing structural periodicity, have received considerable research attention in the past two decades due to their potential for tailoring the elastic/acoustic wave propagation. Theoretical [Sigalas and Economou, 1992; Kushwaha *et al.*, 1993; Sigalas and Economou, 1993] and experimental [de Espinosa *et al.*, 1998; Liu *et al.*, 2000; Vasseur *et al.*, 2001] studies have demonstrated the existence of band gaps in the elastic/acoustic wave band structure of PCs. Acoustic/elastic waves with frequencies within the band gaps are completely forbidden from propagating in the PC. Besides band gaps,

PCs have also shown some other peculiar properties, e.g., negative refraction and sound focusing [Yang *et al.*, 2004; Sukhovich *et al.*, 2008], sub-wavelength imaging [He *et al.*, 2008; Sukhovich *et al.*, 2009] and collimation [Ke *et al.*, 2007; Liu and Su, 2010]. Band gaps and these peculiar properties confer PCs with great promise for applications in insulating vibration, shielding noise and designing various novel acoustic devices. Recent advances in nanotechnologies have allowed the fabrication and characterization of micro-/nano-scale PCs with hypersonic band gaps, and applications of these hypersonic PCs in phonon engineering, acousto-optical devices, and heat management have been anticipated [Gorishnyy *et al.*, 2007; Jang *et al.*, 2007; Robillard *et al.*, 2007; Gomopoulos *et al.*, 2010; Hopkins *et al.*, 2010; Wen *et al.*, 2010].

It is well known that the interface/surface-to-volume ratio of nanosized materials and structures is very high compared to their bulk counterparts, resulting in remarkable interface/surface effect, which can cause the mechanical and other physical properties of nanosized materials to be size-dependent [Gleiter, 2000; Miller and Shenoy, 2000; Cuenot *et al.*, 2004]. To account for this kind of interface/surface effect in the continuum framework, Gurtin and Murdoch [1975] and Gurtin *et al.* [1998] developed an interface/surface elasticity theory, which has been demonstrated to be capable of reproducing well the results of direct atomic simulations [Miller and Shenoy, 2000]. Some researchers have employed the Gurtin–Murdoch interface/surface elasticity theory to study the interface/surface effect on effective elastic constants of nano composites [Duan *et al.*, 2005] and nanoporous materials [Duan *et al.*, 2006]. In addition, this theory has also been utilized to investigate the interface/surface effect on the elastic wave propagation. Wang [2007, 2008] explored the diffraction of elastic waves by nanosized voids and indicated the significant surface effect. Hasheminejad and Avamohammadi [2009] revealed that interface effect can significantly influence the overall dynamic mechanical properties of nanofiber-reinforced composites.

Recently, some efforts have been devoted to exploring the interface/surface effect on the elastic wave propagation in PCs. The present authors extended the multiple scattering theory (MST) method [Mei *et al.*, 2003] by incorporating the interface/surface elasticity theory and demonstrated the surface effect on elastic wave band structure of 2D PCs [Liu *et al.*, 2012a]. Zhen *et al.* developed a method based on the Dirichlet-to-Neumann map and investigated the interface/surface effect on the band structures of transverse [Zhen *et al.*, 2012] and in-plane [Zhen *et al.*, 2013] waves in 2D PCs. Also, Cai and Wei [2013] studied the interface/surface effect on the dispersion relation of in-plane elastic waves in 2D PCs with solid scatterers using the multiple scattering method. All these investigations manifested that the elastic wave band structure of nanosized PCs can be significantly influenced by the interface/surface effect. Nevertheless, both of the two aforementioned types of methods take advantage of the cylindrical wave expansion of the wave field, and thus for 2D PCs only circular cylindrical scatterers can be dealt with, which greatly limits the application of these two methods. Thus, it is desirable to develop an

alternative method that can account for the interface/surface effect on the elastic wave band structure of 2D PCs with arbitrary-shaped scatterers. In this respect, the finite element method shows great potential due to its inherent capability of accommodating complex geometries. Actually finite element schemes based on the interface/surface elasticity theory have already been proposed to model the interface/surface effect on the effective elastic properties of nano inhomogeneous materials [Gao *et al.*, 2006; Tian and Rajapakse, 2007; Yvonnet *et al.*, 2008].

In this paper, based on the Gurtin–Murdoch interface/surface elasticity theory we present a finite element formulation for characterizing the interface/surface effect on the elastic wave propagation in 2D nano PCs. This interface/surface element is subsequently incorporated into the finite element procedure for calculating the elastic wave band structure of PCs. As numerical examples, elastic wave band structures of 2D PCs comprising a square array of circular or elliptical cylindrical nanoholes embedded in an aluminum matrix are calculated and discussed.



## 2. Basic Equations

Consider elastic wave propagation in two-dimensional heterogeneous materials consisting of the matrix and the inclusion of different materials, as schematically represented in Fig. 1. $\Gamma$ denotes the interface between the matrix $\Omega^1$ and the inclusion $\Omega^2$. $\mathbf{n}$ is the unit normal vector to the interface $\Gamma$, with positive $\mathbf{n}$ pointing from $\Omega^2$ to $\Omega^1$. Prescribed tractions $\bar{\mathbf{T}}$ are imposed on external boundary $\partial\Omega_T$ and prescribed displacements $\bar{\mathbf{u}}$ on boundary $\partial\Omega_u$. The equations of motion and the boundary conditions for the matrix and the inclusion are

$$\nabla \cdot \boldsymbol{\sigma} + \mathbf{f} = \rho \ddot{\mathbf{u}}, \tag{1}$$

$$\begin{cases} \mathbf{u} = \bar{\mathbf{u}} & (\text{on } \partial\Omega_u) \\ \boldsymbol{\sigma} \cdot \bar{\mathbf{n}} = \bar{\mathbf{T}} & (\text{on } \partial\Omega_T) \end{cases}, \tag{2}$$

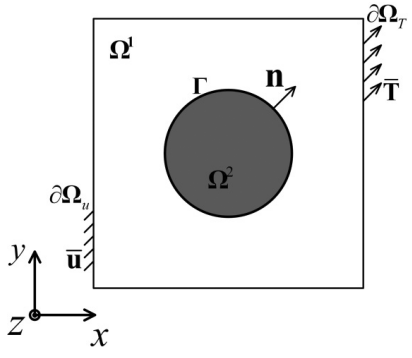


Fig. 1. Sketch of an inhomogeneous material comprising a matrix and an inclusion.

where $\boldsymbol{\sigma}$ is the stress field in $\Omega^1$ or $\Omega^2$, $\mathbf{u}$ is the displacement filed, $\mathbf{f}$ is the body force per unit volume, $\rho$ is the mass density and $\bar{\mathbf{n}}$ is the unit normal vector to the external boundary. The matrix and the inclusion are assumed to be linearly elastic and the infinitesimal strain condition is assumed.

According to the interface/surface elasticity theory, a coherent interface/surface is taken as a negligibly thin elastic continuum which adheres to the abutting bulk materials without slipping. The material properties differ from those of the bulk materials. The equilibrium equation of the interface $\Gamma$ is of following form [Gurtin *et al.*, 1998]:

$$(\boldsymbol{\sigma}^1 - \boldsymbol{\sigma}^2) \cdot \mathbf{n} = -\nabla_s \cdot \boldsymbol{\sigma}_s, \tag{3}$$

where $\boldsymbol{\sigma}^i\,(i = 1, 2)$ is the stress field in $\Omega^i$. $\nabla_s \cdot \boldsymbol{\sigma}_s$ represents the interface/surface divergence of the interface/surface stress $\boldsymbol{\sigma}_s$. For a linear elastically isotropic interface/surface, the constitutive equation reads [Gurtin and Murdoch, 1975; Gurtin *et al.*, 1998]

$$\boldsymbol{\sigma}_s = \lambda_s(\mathrm{tr}\boldsymbol{\varepsilon}_s)\mathbf{I}^{(2)} + 2\mu_s\boldsymbol{\varepsilon}_s, \tag{4}$$

where $\lambda_s$ and $\mu_s$ are the interface/surface elastic constants; $\mathbf{I}^{(2)}$ is the second-rank unit tensor in two-dimensional space; $\boldsymbol{\varepsilon}^s$ is the interface/surface strain, which for a coherent interface/surface equals to the tangential strain of the bulk materials at the interface/surface [Gurtin *et al.*, 1998], i.e.,

$$\varepsilon_s = \mathbf{P} \cdot \boldsymbol{\varepsilon} \cdot \mathbf{P} = \frac{1}{2}\mathbf{P} \cdot [\nabla\mathbf{u} + (\nabla\mathbf{u})^T] \cdot \mathbf{P}, \tag{5}$$

where $\boldsymbol{\varepsilon}$ is the bulk strain and $\mathbf{P} = \mathbf{I} - \mathbf{n} \otimes \mathbf{n}$.

## 3. Formulation of the Interface/Surface Element

Applying the principle of virtual work separately to the matrix and the inclusion gives the following weak forms:

$$\int_{\Omega^1} \delta\boldsymbol{\varepsilon} : \boldsymbol{\sigma} d\Omega = \int_{\Omega^1} \delta\mathbf{u} \cdot (\mathbf{f} - \rho\ddot{\mathbf{u}}) d\Omega - \int_{\Gamma} \delta\mathbf{u} \cdot \boldsymbol{\sigma}^1 \cdot \mathbf{n} dS + \int_{\partial\Omega_T} \delta\mathbf{u} \cdot \bar{\mathbf{T}} dS \tag{6}$$

and

$$\int_{\Omega^2} \delta\boldsymbol{\varepsilon} : \boldsymbol{\sigma} d\Omega = \int_{\Omega^2} \delta\mathbf{u} \cdot (\mathbf{f} - \rho\ddot{\mathbf{u}}) d\Omega + \int_{\Gamma} \delta\mathbf{u} \cdot \boldsymbol{\sigma}^2 \cdot \mathbf{n} dS, \tag{7}$$

where $\delta\mathbf{u}$ is the virtual displacement and $\delta\boldsymbol{\varepsilon}$ is the corresponding virtual strain. Adding Eqs. (6) and (7) together yields

$$\int_{\Omega} \delta\mathbf{u} \cdot \rho\ddot{\mathbf{u}} d\Omega + \int_{\Omega} \delta\boldsymbol{\varepsilon} : \boldsymbol{\sigma} d\Omega + \int_{\Gamma} \delta\mathbf{u} \cdot (\boldsymbol{\sigma}^1 - \boldsymbol{\sigma}^2) \cdot \mathbf{n} dS = \int_{\Omega} \delta\mathbf{u} \cdot \mathbf{f} d\Omega + \int_{\partial\Omega_T} \delta\mathbf{u} \cdot \bar{\mathbf{T}} dS, \tag{8}$$

where $\Omega = \Omega^1 \cup \Omega^2$. By virtue of the equilibrium equation of the interface in (3), (8) can be recast into the following form:

$$\int_\Omega \delta\mathbf{u} \cdot \rho\ddot{\mathbf{u}} d\Omega + \int_\Omega \delta\boldsymbol{\varepsilon} : \boldsymbol{\sigma} d\Omega - \int_\Gamma \delta\mathbf{u} \cdot (\nabla_s \cdot \boldsymbol{\sigma}_s) dS = \int_\Omega \delta\mathbf{u} \cdot \mathbf{f} d\Omega + \int_{\partial\Omega_T} \delta\mathbf{u} \cdot \bar{\mathbf{T}} dS. \tag{9}$$

For closed interface/surface, the following relation can be obtained [Gurtin *et al.*, 1998]

$$\int_\Gamma \delta\mathbf{u} \cdot (\nabla_s \cdot \boldsymbol{\sigma}_s) dS = -\int_\Gamma \delta\varepsilon_s : \boldsymbol{\sigma}_s dS. \tag{10}$$

Substituting (10) into (9) gives

$$\int_\Omega \delta\mathbf{u} \cdot \rho\ddot{\mathbf{u}} d\Omega + \int_\Omega \delta\boldsymbol{\varepsilon} : \boldsymbol{\sigma} d\Omega + \int_\Gamma \delta\boldsymbol{\varepsilon}_s : \boldsymbol{\sigma}_s dS = \int_\Omega \delta\mathbf{u} \cdot \mathbf{f} d\Omega + \int_{\partial\Omega_T} \delta\mathbf{u} \cdot \bar{\mathbf{T}} dS. \tag{11}$$

As per the conventions of the finite element method, it is convenient to rewrite Eq. (11) into the following vectorial form:

$$\int_\Omega \rho\delta\mathbf{u}^T \ddot{\mathbf{u}} d\Omega + \int_\Omega \delta\boldsymbol{\varepsilon}^T \mathbf{D}\boldsymbol{\varepsilon} d\Omega + \int_\Gamma \delta\boldsymbol{\varepsilon}_s^T \mathbf{D}_s \boldsymbol{\varepsilon}_s dS = \int_\Omega \delta\mathbf{u}^T \mathbf{f} d\Omega + \int_{\partial\Omega_T} \delta\mathbf{u}^T \bar{\mathbf{T}} dS, \tag{12}$$

where the superscript $T$ denotes the transpose. $\mathbf{D}$ and $\mathbf{D}_s$ are the linear elasticity matrices of the bulk materials and that of the interface/surface, respectively, which will be given in the following.

Here, in the present work, we use two-dimensional linear elements (either triangular or quadrilateral) to discretize the matrix and the inclusion, while the interface/surface is discretized into two-node linear line elements. The schematic representation of the finite element mesh scheme is depicted in Fig. 2.

Taking advantage of the finite element approximation, the displacement in the bulk elements and that in the interface/surface elements can be expressed as

$$\mathbf{u} = \mathbf{N}\mathbf{a}^e; \quad \mathbf{u} = \mathbf{N}_s \mathbf{a}_s^e, \tag{13}$$

where $\mathbf{N}$ and $\mathbf{N}_s$ are shape function matrices of the matrix/inclusion elements and the interface/surface elements respectively; $\mathbf{a}^e$ and $\mathbf{a}_s^e$ are nodal displacement vectors of the matrix/inclusion elements and the interface/surface elements, respectively. Similarly, the bulk strain and the interface/surface strain can be obtained as

$$\boldsymbol{\varepsilon} = \mathbf{B}\mathbf{a}^e; \quad \boldsymbol{\varepsilon}_s = \mathbf{B}_s \mathbf{a}_s^e, \tag{14}$$

where $\mathbf{B}$ and $\mathbf{B}_s$ are the strain–displacement matrices of the bulk elements and the interface/surface elements, respectively.

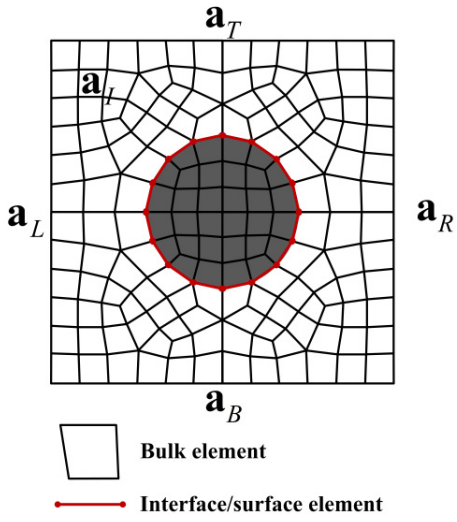


Fig. 2. Schematic representation of the finite element mesh consisting of bulk (matrix and inclusion) elements and interface/surface elements.

Substitution of Eqs. (13) and (14) into (12) yields

$$\sum_e (\delta\mathbf{a}^e)^T\mathbf{M}^e\ddot{\mathbf{a}}^e + \sum_e (\delta\mathbf{a}^e)^T\mathbf{K}^e\mathbf{a}^e + \sum_e (\delta\mathbf{a}_s^e)^T\mathbf{K}_s^e\mathbf{a}_s^e = \sum_e (\delta\mathbf{a}^e)^T\mathbf{P}_f^e + \sum_e (\delta\mathbf{a}^e)^T\mathbf{P}_T^e, \tag{15}$$

where $\mathbf{M}^e$ and $\mathbf{K}^e$ are the mass matrix and the stiffness matrix of the bulk element, respectively; $\mathbf{K}_s^e$ is the stiffness matrix of the interface/surface element; $\mathbf{P}_f^e$ and $\mathbf{P}_T^e$ are the equivalent nodal load vectors,

$$\mathbf{M}^e = \rho\int_{\Omega^e}\mathbf{N}^T\mathbf{N}d\Omega; \quad \mathbf{K}^e = \int_{\Omega^e}\mathbf{B}^T\mathbf{D}\mathbf{B}d\Omega; \quad \mathbf{K}_s^e = \int_{\Gamma^e}\mathbf{B}_s^T\mathbf{D}_s\mathbf{B}_s dS$$

$$\mathbf{P}_f^e = \int_{\Omega^e}\mathbf{N}^T\mathbf{f}d\Omega; \quad \mathbf{P}_T^e = \int_{\partial\Omega_T^e}\mathbf{N}^T\bar{\mathbf{T}}dS.$$

From Eq. (15), the following finite element equation can be derived as

$$\mathbf{M}\ddot{\mathbf{a}} + \mathbf{K}\mathbf{a} = \mathbf{F}, \tag{16}$$

where $\mathbf{K}$ is the stiffness matrix of the matrix/inclusion system obtained by assembling the element stiffness matrices; $\mathbf{M}$ and $\mathbf{F}$ are the total mass matrix and nodal load vectors, respectively.

Assuming two-dimensional elastic wave propagation in the $xy$ plane, all the field variables are invariant along the $z$-axis. The propagation of two-dimensional elastic wave can be decoupled into two modes: in-plane mode and out-of-plane mode.

The bulk strain can be related to the displacement as following:

$$\boldsymbol{\varepsilon} = \{\varepsilon_x \;\; \varepsilon_y \;\; \gamma_{xy} \;\; \gamma_{yz} \;\; \gamma_{zx}\}^T = \mathbf{L}\{u_x \;\; u_y \;\; u_z\}^T = \mathbf{Lu}, \tag{17}$$

where

$$\mathbf{L} = \begin{bmatrix} \frac{\partial}{\partial x} & 0 & \frac{\partial}{\partial y} & 0 & 0 \\ 0 & \frac{\partial}{\partial y} & \frac{\partial}{\partial x} & 0 & 0 \\ 0 & 0 & 0 & \frac{\partial}{\partial y} & \frac{\partial}{\partial x} \end{bmatrix}^T.$$

Therefore, the strain–displacement matrix $\mathbf{B}$ can be calculated as

$$\mathbf{B} = \mathbf{LN}. \tag{18}$$

For a linear elastic matrix or inclusion, the elasticity matrix is given by

$$\mathbf{D} = \frac{E(1-\upsilon)}{(1+\upsilon)(1-2\upsilon)} \begin{bmatrix} 1 & \frac{\upsilon}{1-\upsilon} & 0 & 0 & 0 \\ \frac{\upsilon}{1-\upsilon} & 1 & 0 & 0 & 0 \\ 0 & 0 & \frac{1-2\upsilon}{2(1-\upsilon)} & 0 & 0 \\ 0 & 0 & 0 & \frac{1-2\upsilon}{2(1-\upsilon)} & 0 \\ 0 & 0 & 0 & 0 & \frac{1-2\upsilon}{2(1-\upsilon)} \end{bmatrix}, \tag{19}$$

where $E$ and $\upsilon$ are Young's modulus and Poisson's ratio of the matrix or the inclusion, respectively.

The relation between interface/surface strain and bulk strain in Eq. (5) can be expressed in the Cartesian coordinate system as

$$\boldsymbol{\varepsilon}_s = \{\varepsilon^s_{xx} \;\; \varepsilon^s_{yy} \;\; \gamma^s_{xy} \;\; \gamma^s_{xz} \;\; \gamma^s_{yz}\} = \mathbf{H}\boldsymbol{\varepsilon}, \tag{20}$$

where

$$\mathbf{H} = \begin{bmatrix} s^4 & c^2s^2 & -cs^3 & 0 & 0 \\ c^2s^2 & c^4 & -sc^3 & 0 & 0 \\ -2cs^3 & -2sc^3 & 2c^2s^2 & 0 & 0 \\ 0 & 0 & 0 & s^2 & -cs \\ 0 & 0 & 0 & -cs & c^2 \end{bmatrix},$$

where $s = \sin\theta$, $c = \cos\theta$ and $\theta$ is the angle between the out-normal of the interface/surface and the $x$-axis. Thus, the strain–displacement matrix $\mathbf{B}_s$ for the interface/surface can be obtained from Eqs. (13), (14), (17) and (20) as

$$\mathbf{B}_s = \mathbf{HLN}_s. \tag{21}$$

For the two-dimensional elastic wave propagation problem, the elasticity matrix of the interface/surface in the Cartesian coordinate system is of the following form:

$$\mathbf{D}_s = \begin{bmatrix} (\lambda_s + 2\mu_s) & 0 & 0 & 0 & 0 \\ 0 & (\lambda_s + 2\mu_s) & 0 & 0 & 0 \\ 0 & 0 & \frac{1}{2}(\lambda_s + 2\mu_s) & 0 & 0 \\ 0 & 0 & 0 & \mu_s & 0 \\ 0 & 0 & 0 & 0 & \mu_s \end{bmatrix}, \tag{22}$$

where $\lambda_s$ and $\mu_s$ are the interface/surface elastic constants.

With properly chosen shape function matrices $\mathbf{N}$ and $\mathbf{N}_s$, matrices $\mathbf{B}$ and $\mathbf{B}_s$ can be obtained according to Eqs. (18) and (21), respectively. Therefore, the mass matrix and the stiffness matrix embodying the interface/surface effect in Eq. (16) can be obtained. Through Eq. (16), one can investigate the elastic wave propagation in two-dimensional nanosized inhomogeneous materials, like nano PCs, with consideration of the interface/surface effect.



## 4. Finite Element Procedure for Calculation of Elastic Wave Band Structure of PCs

In the present study, primary concern is focused on the interface/surface effect on the elastic wave band structure of 2D nano PCs. The finite element procedure for calculating elastic wave band structures of PCs has already been widely used to explore the band gap characteristics of PCs [Axmann and Kuchment, 1999; Phani *et al.*, 2006; Liu *et al.*, 2012b]. Here, we incorporate the interface/surface element formulated in the previous section and then explore the interface/surface effect on the band structure of nano PCs. For completeness, band structure calculation procedure based on the finite element method is briefly introduced in the following.

In view of Bloch's theorem that characterizes the wave propagation in periodic structures, the wave propagation characteristics of a periodic structure can be revealed by analyzing a unit cell of it. When a plane elastic wave with frequency $\omega$ is propagating within a 2D nano PC, the equations of motion in Eq. (16) for a unit cell in the absence of external forces can be rewritten into the following form:

$$(-\omega^2\mathbf{M} + \mathbf{K})\mathbf{a} = \mathbf{0}. \tag{23}$$

Again according to Bloch's theorem, nodal displacements at the boundaries of the unit cell are not independent. For instance, the following relations can be derived for 2D PCs with square topology [Liu *et al.*, 2012b]

$$\mathbf{a}_R = \mathbf{a}_L \exp(2\pi k_1); \quad \mathbf{a}_T = \mathbf{a}_B \exp(2\pi k_2), \tag{24}$$

where $\mathbf{a}_L$, $\mathbf{a}_R$, $\mathbf{a}_B$ and $\mathbf{a}_T$ signify the nodal displacement vectors of the left, right, bottom and top nodes of the unit cell, as shown in Fig. 2; $k_1$ and $k_2$ are components of the Bloch wave vector $\mathbf{k}$ in the reciprocal space. Equation (24) can be rewritten

into the following compact matrix form:

$$\mathbf{a} = \mathbf{T}\bar{\mathbf{a}}, \tag{25}$$

where

$$\mathbf{T} = \begin{bmatrix} \mathbf{I}\exp(2\pi k_1) & \mathbf{0} & \mathbf{0} \\ \mathbf{0} & \mathbf{I}\exp(2\pi k_2) & \mathbf{0} \\ \mathbf{I} & \mathbf{0} & \mathbf{0} \\ \mathbf{0} & \mathbf{I} & \mathbf{0} \\ \mathbf{0} & \mathbf{0} & \mathbf{I} \end{bmatrix}, \quad \mathbf{a} = \begin{bmatrix} \mathbf{a}_R \\ \mathbf{a}_T \\ \mathbf{a}_L \\ \mathbf{a}_B \\ \mathbf{a}_I \end{bmatrix}, \quad \bar{\mathbf{a}} = \begin{bmatrix} \mathbf{a}_L \\ \mathbf{a}_B \\ \mathbf{a}_I \end{bmatrix},$$

and $\mathbf{a}_I$ is the displacement vector of internal nodes of the unit cell, as shown in Fig. 2. Substituting Eq. (25) into the equations of motion in Eq. (23) yields

$$(-\omega^2\bar{\mathbf{M}} + \bar{\mathbf{K}})\bar{\mathbf{a}} = \mathbf{0}, \tag{26}$$

where $\bar{\mathbf{M}} = \mathbf{T}^H\mathbf{M}\mathbf{T}$, $\bar{\mathbf{K}} = \mathbf{T}^H\mathbf{K}\mathbf{T}$, and the superscript $H$ denotes the Hermitian transpose.

Varying $\mathbf{k} = (k_1, k_2)$ along the periphery of the irreducible part of the first Brillouin zone and solving for the corresponding natural frequencies from Eq. (26), a series of curves of $\omega$ versus $\mathbf{k}$, i.e., the band structure, can be obtained.

## 5. Numerical Results and Discussions

In this section, the surface effect on the elastic wave band structure is demonstrated and discussed by calculating the elastic wave band structures of 2D nano PCs via the band structure calculation procedure equipped with the interface/surface element presented in the previous sections. The 2D PCs considered herein are composed of a square array of circular or elliptical cylindrical nanoholes embedded in an aluminum matrix.

### 5.1. 2*D PCs with circular cylindrical nanoholes*

First, we consider a 2D PC consisting of parallel infinite circular cylindrical nanoholes embedded in an aluminum matrix and arranged in square lattice, which is sketched in Fig. 3(a). The radius of the hole $a$ and the lattice constant $d$ are 4.1 nm and 10 nm, respectively. Thus, the filling ratio $f$ is 0.53. The material parameters of the aluminum matrix include the mass density $\rho = 2697\,\mathrm{kg/m^3}$, Lamé constants $\lambda = 52.09\,\mathrm{GPa}$ and $\mu = 34.7\,\mathrm{GPa}$. Two sets of surface elastic constants which were obtained by Miller and Shenoy [2000] via molecular dynamics simulation are employed to characterize the surface effect: $\lambda_s = 3.489\,\mathrm{N/m}$, $\mu_s = -6.218\,\mathrm{N/m}$ (denoted as surface property A); $\lambda_s = 6.842\,\mathrm{N/m}$, $\mu_s = -0.376\,\mathrm{N/m}$ (denoted as surface property B). The discretization of a unit cell is presented in Fig. 3(b), where the aluminum matrix is discretized into 5510 4-node quadrilateral elements while

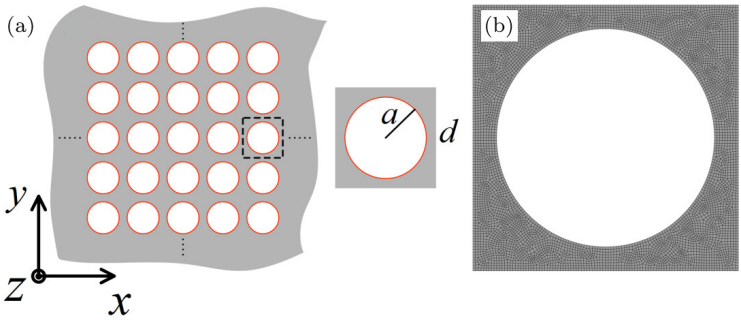


Fig. 3. (a) Sketch of the 2D PC consisting of a square array of circular cylindrical nanoholes embedded in an aluminum matrix, and (b) the finite element discretization of a unit cell.



the surface is discretized into 256 2-node line surface elements. It has been verified but not detailed here that this mesh density is enough to generate converged band structure results.

As stated previously, the elastic wave propagation within 2D PCs can be decoupled into two types of modes: the in-plane mode polarized in the $x$–$y$ plane and the out-of-plane mode polarized in the $z$-axis. For clarity, the band structures of the 2D PCs with circular nanoholes are presented separately for the in-plane mode and the out-of-plane mode. Illustrated in Fig. 4 are the band structures for the in-plane mode and those for the out-of-plane mode with and without surface effect,

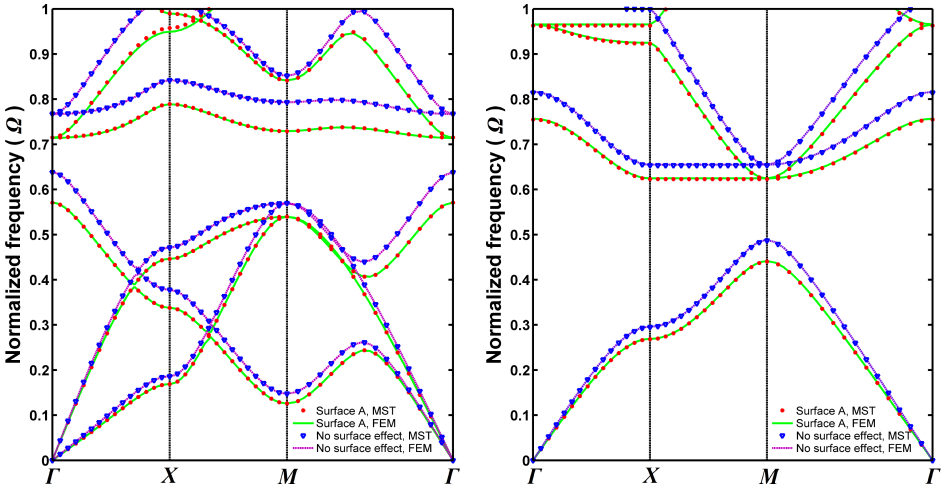


Fig. 4. Band structures of the 2D square PC with circular cylindrical nanoholes: (a) in-plane mode; (b) out-of-plane mode. Surface property A is considered for the surface effect. Here, and in the following band structure plots, the frequency is normalized by $2\pi C/d$, where $C$ is the shear wave velocity in the matrix. Γ, $X$, and $M$ are the high symmetry points of the irreducible part of the first Brillouin zone.

where the surface property A is considered for the surface effect. In all the band structure plots presented in this paper, the frequency on the $y$-axis is normalized as $\mathbf{\Omega} = \omega \cdot d/2\pi C$, where $C$ is the shear wave velocity in the matrix. For the sake of comparison, results obtained using both the present finite element procedure and the MST method [Liu *et al.*, 2012a] are depicted together in Fig. 4.

From Fig. 4, it can be clearly observed that the results obtained using the finite element procedure in this paper is in good agreement with those obtained using the MST method, no matter the surface effect is considered or not, which speaks well for the capability of the interface/surface element to account for the interface/surface effect on the elastic wave band structure. It is also manifested in Fig. 4 that the surface effect on the elastic wave band structure is remarkable, especially in the relatively high frequency regime. In Fig. 4, all the frequency bands shift downwards due to the surface effect described by the surface property A. For the in-plane mode case shown in Fig. 4(a), there is a complete band gap extending from the normalized frequency 0.6407–0.7692 when surface effect is ignored, nevertheless the band gap shifts to being from 0.5839 to 0.7294 if the surface effect is taken into account, i.e., the first band gap for the in-plane mode becomes lower and wider due to the surface effect. Similarly, in Fig. 4(b) for the out-of-plane mode, frequency bands also become lower. The first complete band gap for the out-of-plane mode also becomes wider as the surface effect described by the surface A is considered. It extends from 0.4881 to 0.6523 without the surface effect, while it becomes from 0.4419 to 0.6225 as the surface effect is accounted for.

Figure 5 depicts the band structures for the in-plane mode and those for the out-of-plane mode with the surface property B being considered for the surface effect.

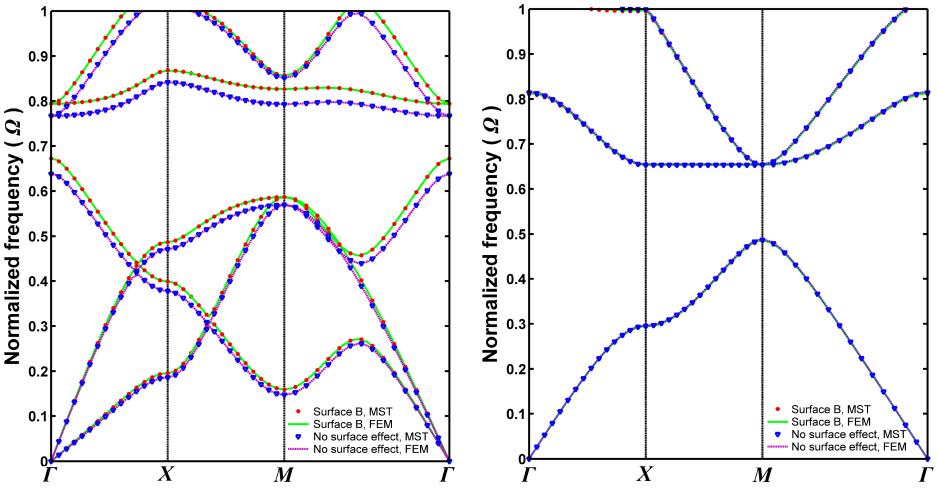


Fig. 5. Band structures of the 2D square PC with circular cylindrical nanoholes: (a) in-plane mode; (b) out-of-plane mode. Surface property B is considered for the surface effect.

Again, in Fig. 5(a) one can easily observe that the present finite element procedure and the MST method generate coincident results which indicate the significant surface effect on the elastic wave band structure for the in-plane mode. However, the frequency bands in Fig. 5(a) shift upwards due to the surface effect described by the surface property B. In addition, the first complete band gap becomes higher and narrower with the surface effect being considered, extending from 0.6805 to 0.8011. These observations are different from those in Fig. 4(a).

It has been found [Liu *et al.*, 2012a] in the formulation of the MST method that the interface/surface effect on the elastic wave band structure of 2D nano PCs with circular holes can be characterized by two dimensionless parameters: $k_1 = (\lambda_s + 2\mu_s)/(\mu_1 a)$ for the in-plane mode, and $k_2 = \mu_s/(\mu_1 a)$ for the out-of-plane mode, where $\mu_1$ is the shear modulus of the matrix. For the surface property A, both $k_1$ and $k_2$ are negative, which has been demonstrated to result in decrease in the in-plane bulk and shear moduli as well as the out-of-plane shear modulus of 2D nanoporous materials, i.e., surface with property A is a kind of "soft" surface [Duan *et al.*, 2006]. In contrast, for surface property B, $k_1$ is positive, indicating surface with property B is "stiff" in the sense of in-plane moduli. From Figs. 4 and 5(a), it seems that the "soft" surfaces lower the frequency bands of 2D nano PCs and slightly widen the first band gap, while the "stiff" surfaces cause the frequency bands to become higher and meanwhile slightly narrow the first band gap. Similar observations have also been reported by Zhen *et al.* [2012, 2013].

It should be noted in Fig. 5(b) that in the normalized frequency range 0–1, the difference between the results with and without surface effect is small compared to those in Figs. 4 and 5(a). It can be understood from the fact that for surface property B, the surface elastic constant $\mu_s$ is considerably small, resulting in a small value of $k_2$, and thus the surface effect on the band structure for the out-of-plane mode is tiny here.

### 5.2. 2D PCs with elliptical cylindrical nanoholes

As mentioned in the introduction, currently interface/surface effect on the elastic wave band structure can be analyzed via the existing methods only for 2D nano PCs with circular cylindrical scatterers [Liu *et al.*, 2012a; Zhen *et al.*, 2012; Cai and Wei, 2013; Zhen *et al.*, 2013]. In contrast, thanks to the inherent advantage of the finite element method to accommodate complex geometries, there is no apparent restriction on the shape of scatterers when the finite element procedure presented in this paper to characterize the interface/surface effect is used. In this subsection, band structures of 2D PCs consisting of a square array of elliptical cylindrical nanoholes embedded in an aluminum matrix are presented. The 2D PCs with elliptical cylindrical nano holes are schematically depicted in Fig. 6, where $a$ and $b$ denote the semi-major axis and semi-minor axis, respectively. The lattice constant $d$ is again set to be 10 nm. Now we keep the filling ratio of the scatterer (0.53) unchanged, and vary $a$ (and correspondingly $b$) to examine the variation of the interface/surface

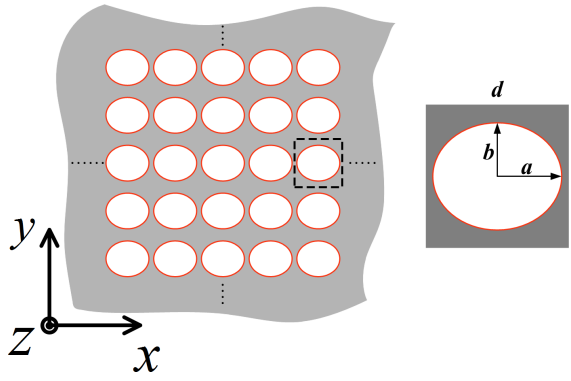


Fig. 6. Sketch of 2D PCs consisting of a square array of elliptical cylindrical nanoholes embedded in an aluminum matrix.



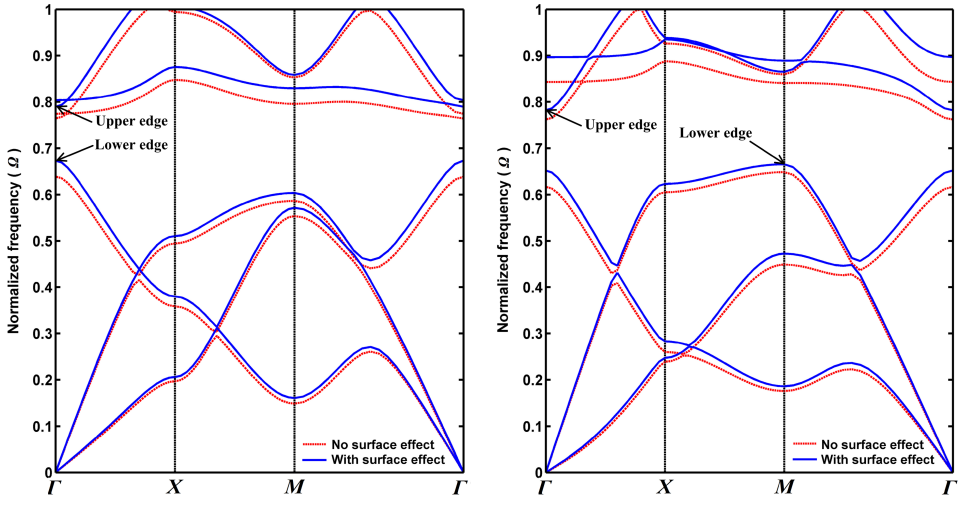


Fig. 7. Band structures of 2D square PCs with elliptical cylindrical nanoholes for the in-plane mode: (a) $e = 0.3031$; (b) $e = 0.6488$. Surface property B is considered for the surface effect.

effect. The eccentricity of the ellipse defined as $e = \sqrt{(a^2 - b^2)/a^2}$ is employed to quantitatively describe the sectional shape change of the scatterer. The material properties of the matrix are identical to those in Sec. 5.1.

Figure 7 shows the band structures of 2D PCs with elliptical cylindrical nanoholes for the in-plane mode, where in Fig. 7(a) the eccentricity $e = 0.3031$ and in Fig. 7(b) $e = 0.6488$. The surface property B is considered in the calculation. In Fig. 7, it is clearly evidenced that the surface effect on the band structure can be significant for 2D nano PCs with noncircular cylindrical scatterers. And the frequency bands become higher due to the "stiff" surface with property B.

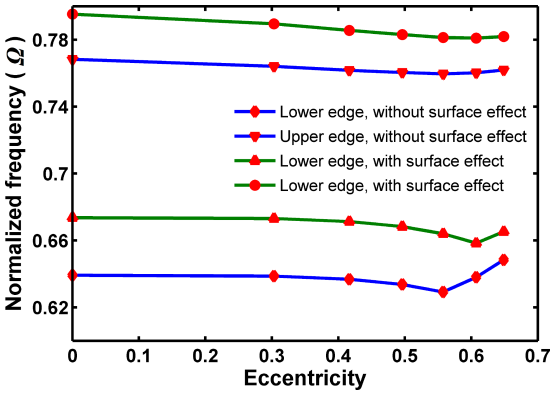


Fig. 8. Variation of the upper and lower edges of the first band gap with the eccentricity for 2D square PCs with elliptical cylindrical nanoholes for the in-plane mode. Surface property B is considered for the surface effect.



Figure 8 illustrates the variations of the upper and lower edges of the first band gap for the in-plane mode with the eccentricity $e$ of the scatterer, where $e = 0$ corresponds the results of 2D PCs with circular cylindrical nanoholes. Figure 8 indicates that both the lower edge and the upper edge first decrease slightly with increasing eccentricity and then increase with further increasing eccentricity. The more obvious increase of the lower edge for large eccentricities can be intuitively understood by closely examining the band structures presented in Fig. 7. For the case of a smaller $e = 0.3031$ in Fig. 7(a), it is noted that, both the lower and upper edge are located at the high symmetry point $\mathbf{\Gamma}$. Nevertheless, Fig. 7(b) shows that, for the case of a larger $e = 0.6488$, the upper edge remains at $\mathbf{\Gamma}$ point, while the lower edge shifts to the high symmetry point $\mathbf{M}$. This shift is primarily due to the shape change of the scatterer. However, close examination of Fig. 8 indicates

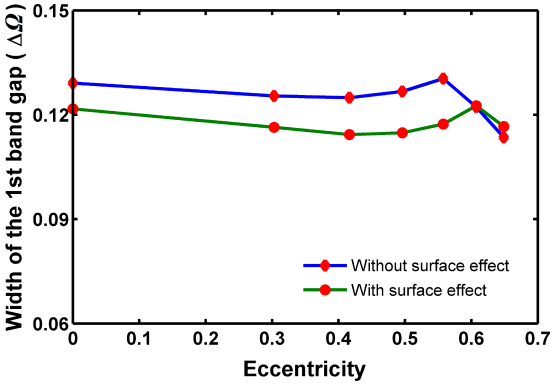


Fig. 9. Variation of the width of the first band gap with the eccentricity for 2D square PCs with elliptical cylindrical nanoholes for the in-plane mode. Surface property B is considered for the surface effect.

that the shift of the lower edge from $\mathbf{\Gamma}$ point to $\mathbf{M}$ point happens at $e = 0.5576$ if the surface effect is not considered, while this shift would happen at $e = 0.6074$ if the surface effect is present, which demonstrates the surface effect on the band gap characteristics of 2D nano PCs with noncircular scatterers. The variation in the width of the first band gap for the in-plane mode with the eccentricity $e$ of the scatterer is depicted in Fig. 9. It is seen that for small eccentricities the surface effect described by the surface property B slightly narrows the first band gap, while for large eccentricities this narrowing phenomenon is much less obvious.

## 6. Conclusion

In summary, an interface/surface element is formulated based on the Curtin–Murdoch interface/surface elasticity theory for accounting the interface/surface effect on the elastic wave propagation in 2D nano PCs. This interface/surface element is incorporated into the finite element procedure for calculating the elastic wave band structure of 2D nano PCs. The capability of the interface/surface element is validated through the good agreement between the band structures of a 2D PC with circular cylindrical nanoholes obtained by using the MST method and those obtained by using the present finite element procedure. As an advantage over the existing methods, the ability of the present procedure in treating 2D PCs with noncircular cylindrical scatterers has also been demonstrated by calculations of band structures of 2D PCs comprising a square array of elliptical cylindrical nanoholes embedded in an aluminum matrix. Numerical results presented in this paper clearly evidence that the interface/surface effect on the elastic wave band structure can be significant as the characteristic size of PCs shrinks to nanometers.



## Acknowledgment

The authors are grateful for the support by the National Natural Science Foundation of China under Grant No. 11232001.

## References

Axmann, W. and Kuchment, P. [1999] "An efficient finite element method for computing spectra of photonic and acoustic band-gap materials: I. Scalar case," *Journal of Computational Physics* **150**(2), 468–481.

Cai, B. and Wei, P. J. [2013] "Surface/interface effects on dispersion relations of 2D phononic crystals with parallel nanoholes or nanofibers," *Acta Mechanica* **224**(11), 2749–2758.

Cuenot, S., Fretigny, C., Demoustier-Champagne, S. and Nysten, B. [2004] "Surface tension effect on the mechanical properties of nanomaterials measured by atomic force microscopy," *Physical Review B* **69**(16), 165410.

de Espinosa, F. M., Jimenez, E. and Torres, M. [1998] "Ultrasonic band gap in a periodic two-dimensional composite," *Physical Review Letters* **80**(6), 1208–1211.

Duan, H. L., Wang, J., Huang, Z. P. and Karihaloo, B. L. [2005] "Size-dependent effective elastic constants of solids containing nano-inhomogeneities with interface stress," *Journal of Mechanics and Physics of Solids* **53**(7), 1574–1596.

Duan, H. L., Wang, J., Karihaloo, B. L. and Huang, Z. [2006] "Nanoporous materials can be made stiffer than non-porous counterparts by surface modification," *Acta Materialia* **54**(11), 2983–2990.

Gao, W., Yu, S. W. and Huang, G. Y. [2006] "Finite element characterization of the size-dependent mechanical behaviour in nanosystems," *Nanotechnology* **17**(4), 1118–1122.

Gleiter, H. [2000] "Nanostructured materials: Basic concepts and microstructure," *Acta Materialia* **48**(1), 1–29.

Gomopoulos, N., Maschke, D., Koh, C., Thomas, E., Tremel, W., Butt, H.-J. and Fytas, G. [2010] "One-dimensional hypersonic phononic crystals," *Nano Letters* **10**(3), 980–984.

Gorishnyy, T., Jang, J. H., Koh, C. and Thomas, E. L. [2007] "Direct observation of a hypersonic band gap in two-dimensional single crystalline phononic structures," *Applied Physics Letters* **91**(12), 121915.

Gurtin, M. E. and Murdoch, A. I. [1975] "A continuum theory of elastic material surfaces," *Archive for Rational Mechanics and Analysis* **57**(4), 291–323.

Gurtin, M. E., Weissmuller, J. and Larche, F. [1998] "A general theory of curved deformable interfaces in solids at equilibrium," *Philosophical Magazine A* **78**(5), 1093–1109.

Hasheminejad, S. M. and Avamohammadi, R. [2009] "Size-dependent effective dynamic properties of unidirectional nanocomposites with interface energy effects," *Composites Science and Technology* **69**(15–16), 2538–2546.

He, Z. J., Cai, F. Y., Ding, Y. Q. and Liu, Z. Y. [2008] "Subwavelength imaging of acoustic waves by a canalization mechanism in a two-dimensional phononic crystal," *Applied Physics Letters* **93**(23), 233503.

Hopkins, P. E., Reinke, C. M., Su, M. F., Olsson III, R. H., Shaner, E. A., Leseman, Z. C., Serrano, J. R., Phinney, L. M. and El-Kady, I. [2010] "Reduction in the thermal conductivity of single crystalline silicon by phononic crystal patterning," *Nano Letters* **11**(1), 107–112.

Jang, J. H., Ullal, C. K., Maldovan, M., Gorishnyy, T., Kooi, S., Koh, C. Y. and Thomas, E. L. [2007] "3D micro- and nanostructures via interference lithography," *Advanced Functional Materials* **17**(16), 3027–3041.

Ke, M. Z., Liu, Z. Y., Pang, P., Qiu, C. Y., Zhao, D. G., Peng, S. S., Shi, J. and Wen, W. J. [2007] "Experimental demonstration of directional acoustic radiation based on two-dimensional phononic crystal band edge states," *Applied Physics Letters* **90**(8), 083509.

Kushwaha, M. S., Halevi, P., Dobrzynski, L. and Djafarirouhani, B. [1993] "Acoustic band-structure of periodic elastic composites," *Physical Review Letters* **71**(13), 2022–2025.

Liu, W., Chen, J. W., Liu, Y. Q. and Su, X. Y. [2012a] "Effect of interface/surface stress on the elastic wave band structure of two-dimensional phononic crystals," *Physical Review Letters A* **376**(4), 605–609.

Liu, W., Chen, J. W. and Su, X. Y. [2012b] "Local resonance phononic band gaps in modified two-dimensional lattice materials," *Acta Mechanica Sinica* **28**(3), 659–669.

Liu, W. and Su, X. Y. [2010] "Collimation and enhancement of elastic transverse waves in two-dimensional solid phononic crystals," *Physics Letters A* **374**(29), 2968–2971.

Liu, Z. Y., Zhang, X. X., Mao, Y. W., Zhu, Y. Y., Yang, Z. Y., Chan, C. T. and Sheng, P. [2000] "Locally resonant sonic materials," *Science* **289**(5485), 1734–1736.

Mei, J., Liu, Z. Y., Shi, J. and Tian, D. C. [2003] "Theory for elastic wave scattering by a two-dimensional periodical array of cylinders: An ideal approach for band-structure calculations," *Physical Review B* **67**(24), 245107.

Miller, R. E. and Shenoy, V. B. [2000] "Size-dependent elastic properties of nanosized structural elements," *Nanotechnology* **11**(3), 139–147.

Phani, A. S., Woodhouse, J. and Fleck, N. A. [2006] "Wave propagation in two-dimensional periodic lattices," *Journal of the Acoustical Society of America* **119**(4), 1995–2005.

Robillard, J. F., Devos, A. and Roch-Jeune, I. [2007] "Time-resolved vibrations of two-dimensional hypersonic phononic crystals," *Physical Review B* **76**(9), 092301.

Sigalas, M. and Economou, E. N. [1993] "Band-structure of elastic-waves in 2-dimensional systems," *Solid State Communications* **86**(3), 141–143.

Sigalas, M. M. and Economou, E. N. [1992] "Elastic and acoustic-wave band-structure," *Journal of Sound and Vibration* **158**(2), 377–382.

Sukhovich, A., Jing, L. and Page, J. H. [2008] "Negative refraction and focusing of ultrasound in two-dimensional phononic crystals," *Physical Review B* **77**(1), 014301.

Sukhovich, A., Merheb, B., Muralidharan, K., Vasseur, J. O., Pennec, Y., Deymier, P. A. and Page, J. H. [2009] "Experimental and theoretical evidence for subwavelength imaging in phononic crystals," *Physical Review Letters* **102**(15), 154301.

Tian, L. and Rajapakse, R. K. N. D. [2007] "Finite element modelling of nanoscale inhomogeneities in an elastic matrix," *Computational Materials Science* **41**(1), 44–53.

Vasseur, J. O., Deymier, P. A., Chenni, B., Djafari-Rouhani, B., Dobrzynski, L. and Prevost, D. [2001] "Experimental and theoretical evidence for the existence of absolute acoustic band gaps in two-dimensional solid phononic crystals," *Physical Review Letters* **86**(14), 3012–3015.

Wang, G. F. [2007] "Diffraction of plane compressional wave by a nanosized spherical cavity with surface effects," *Applied Physics Letters* **90**(21), 211907.

Wang, G. F. [2008] "Diffraction of shear waves by a nanosized spherical cavity," *Journal of Applied Physics* **103**(5), 053519.

Wen, Y.-C., Sun, J.-H., Dais, C., Grutzmacher, D., Wu, T.-T., Shi, J.-W. and Sun, C.-K. [2010] "Three-dimensional phononic nanocrystal composed of ordered quantum dots," *Applied Physics Letters* **96**(12), 123113.

Yang, S. X., Page, J. H., Liu, Z. Y., Cowan, M. L., Chan, C. T. and Sheng, P. [2004] "Focusing of sound in a 3D phononic crystal," *Physical Review Letters* **93**(2), 024301.

Yvonnet, J., Le Quang, H. and He, Q. C. [2008] "An XFEM/level set approach to modelling surface/interface effects and to computing the size-dependent effective properties of nanocomposites," *Computational Mechanics* **42**(1), 119–131.

Zhen, N., Wang, Y. S. and Zhang, C. Z. [2012] "Surface/interface effect on band structures of nanosized phononic crystals," *Mechanics Research Communications* **46**, 81–89.

Zhen, N., Wang, Y. S. and Zhang, C. Z. [2013] "Bandgap calculation of in-plane waves in nanoscale phononic crystals taking account of surface/interface effects," *Physica E: Low-dimensional Systems and Nanostructures* **54**, 125–132.